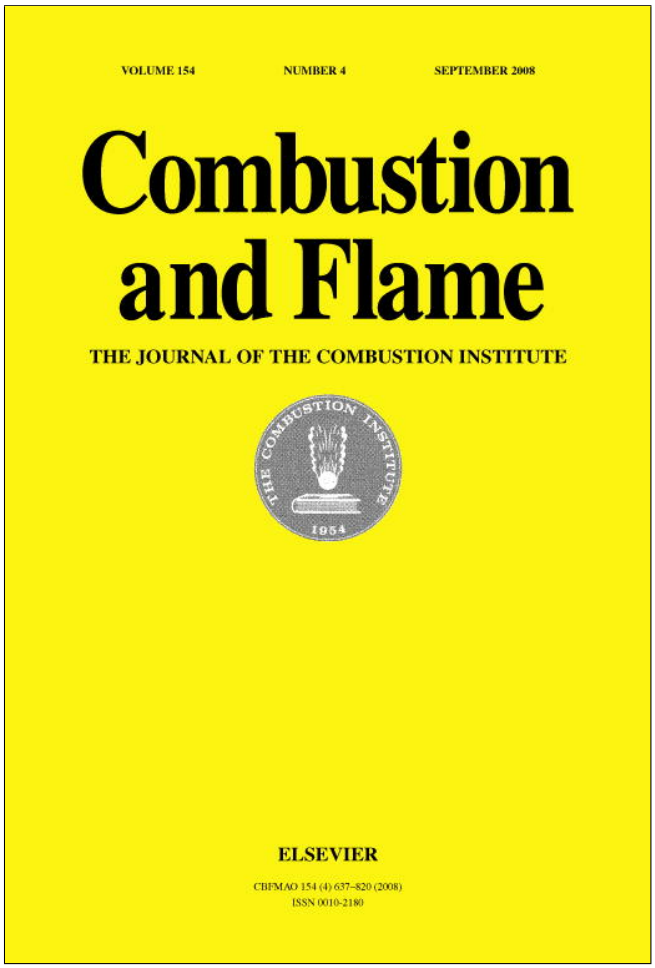

Available online at www.sciencedirect.com
ScienceDirect
Combustion and Flame 154 (2008) 789–801
Combustion and Flame
www.elsevier.com/locate/combustflame

Microgravity opposed-flow flame spread in polyvinyl chloride tubes

George W. Sidebotham [a,*], Sandra L. Olson [b]

[a] *Mechanical Engineering Department, The Cooper Union for the Advancement of Science and Art, 51 Astor Place, New York, NY 10003, USA*

[b] *NASA Glenn Research Center, Cleveland, OH 44135-3191, USA*

Received 11 October 2007; received in revised form 11 April 2008; accepted 25 May 2008

Available online 28 June 2008

Abstract

The effects of gravity on opposed-flow flame spread in a confined geometry were investigated experimentally in the 2.2-s drop tower at the NASA Glenn Research Center. Pure oxygen flowed through samples of 0.64-cm-inner-diameter polyvinyl chloride (PVC) tubing held either horizontally or vertically in a combustion chamber filled with nitrogen. The sample was ignited in normal gravity with a hot wire, and once a flame was established, the apparatus was dropped to observe microgravity effects. Flame spread rate was measured in normal and microgravity at pressures of 1.0 and 0.5 atm. A low-flow ignition limit was observed at an opposed-flow velocity of 1.36 cm/s, at which point the horizontal, vertical, and microgravity flame spread rates were 0.40, 0.30, and 0.16 cm/s, respectively. For flow velocities above approximately 5.2 cm/s, there was no difference in the flame spread rates for normal and microgravity and the flame spread rate increased with a nearly square root dependence with respect to opposed-flow velocity. Buoyant flow velocities of 2.5 and 1.5 cm/s were estimated for horizontal and vertical flames, respectively. Vertical tests conducted at 0.5 atm pressure demonstrated no difference in flame spread rate between normal and microgravity. These results suggest that the fire risk associated with the use of PVC tubes during general anesthesia in either space or ground applications may be reduced if the application of a high-energy surgical tool is prevented during an active phase of the breathing cycle (inhale or exhale).

Keywords: Flame spread; Microgravity; Buoyancy; Polyvinyl chloride; Oxygen; Tubing

1. Introduction

As the durations of human missions increase and especially as emergency return to earth becomes impossible, mission plans must include procedures to address medical emergencies in space. Terrestrial surgery frequently involves the simultaneous use of flammable materials (drapes, endotracheal tubes, intestinal gases), strong oxidizers (oxygen, nitrous oxide), and high-energy surgical tools (lasers, electrocauteries), and there is thus significant fire risk. While rare, operating room fires have been reported [1,2] and it is likely that many unreported fires have occurred. Bruley [3] estimates 100 minor fires and 10 serious fires with one or two fatalities annually in the United States. Previous work in normal gravity

* Corresponding author. Fax: +1 (212) 353 4341.
E-mail address: sidebo@cooper.edu (G.W. Sidebotham).

0010-2180/$ – see front matter
doi:10.1016/j.combustflame.2008.05.014

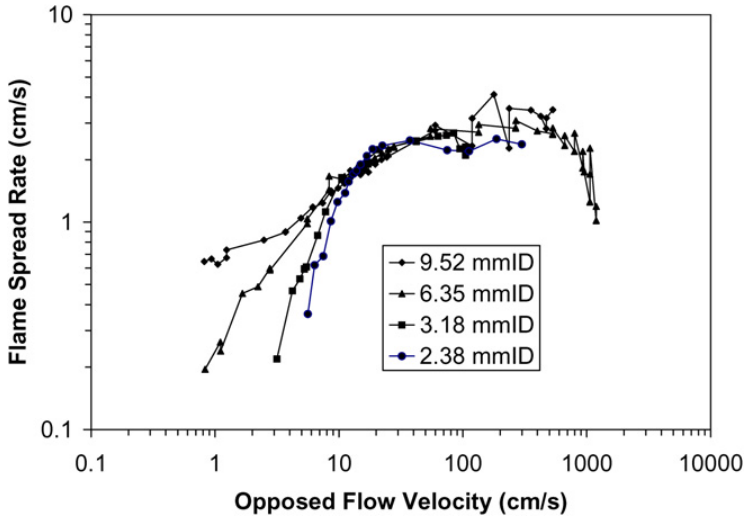

Fig. 1. Data from master's thesis of Stern. Flame spread rate along the inner surface of horizontal clear polyvinyl chloride tubing is plotted against opposed oxygen flow velocity for several tube inner diameters (ID) on logarithmic axes. The end points on the low-flow end are extinction limits. The high-flow extinction limit was tested only for the 6.35-mm-ID tubing. Scatter for higher flows is attributed to the real-time stopwatch measurement of intensely bright flames.

has shown that the accidental ignition of polyvinyl chloride (PVC) endotracheal tubes (breathing tubes used during general anesthesia) by high-energy surgical devices results in an opposed-flow flame that spreads along the inner surface of the tube [4–6]. This primary flame consumes oxygen fed to it and produces fuel gases that can ignite a secondary jet flame. The character of these flames depends strongly on the flow rate and oxygen concentration of oxidizer supplied. Efforts to train astronauts to intubate patients in zero gravity [7] and recognition of the increased fire risk when oxygen is used during intubation [8] reflect the importance of this potential problem to the space industry.

While this work was initially motivated by the surgical fire safety problem, the geometry used for laboratory study provides a simple, reproducible experiment for the fundamental study of flame spread phenomena. An oxidizer flow is established through a flammable solid material in tube form, and an ignition source is applied to the free end, or through a perforation in the tubing (created by a laser, for example). A flame is quickly established and spreads toward the oxidizer source at a measurable velocity.

Fig. 1 shows the normal gravity flame spread rate as a function of oxidizer (pure oxygen) flow rate for several tube inner diameters taken from the master's thesis of Stern [9] for horizontal flames. Borrowing the language of the pioneering work of Fernandez-Pello and co-workers [10,11] for opposed-flow flame spread over PMMA, the data exhibit a buoyant regime (from approximately 1 to 10 cm/s opposing flow velocity), followed by a thermal regime (10 to 100 cm/s), and ending in a chemical regime (100 to 1000 cm/s). In the buoyant regime there is a clear effect of tube diameter. For the largest tube diameter studied (0.95 cm), the effects of buoyantly induced flow are suggested by the inflection point at approximately 4 cm/s. However, for smaller tube diameters, the absence of an inflection point suggests that the effects of buoyancy are reduced as compared to the traditional flame spread against an oxidizer that is infinite in extent. In fact, a low-flow flammability limit can be readily measured with this geometry [12]. To our knowledge, such limits have only been reported in microgravity experiments [13].

In the thermal regime, all four data sets collapse onto a common curve of increasing flame spread rate with increasing opposed-flow velocity. In the chemical regime, the flame spread rate drops with increasing flow. Hashimoto and co-workers [14] observed similar behavior in their study of flame spread using a geometry similar to that in this study within PMMA cylinders. A reduction in peak flame spread rates for diameters below 2 mm was observed for PMMA, which was attributed to curvature effects. Similar effects were seen for diameters of 1.6 mm by Stern [9], and not reported in Fig. 1 due to aberrant transient behavior not observed in larger diameter tubes. The peak flame spread rates for PVC are approximately three times greater than for PMMA, while the range of opposed flow for which these flames exist is nearly identical. Little mention of the low-flow behavior is made in that study, which was motivated by high heat release rate applications.

Opposed-flow flame spread was studied in a rectangular confined geometry by Olson et al. [15]. Air was flown across both sides of filter paper, held horizontally, with a 5-mm gap on both sides. Flames were ignited at a relatively high opposed-flow veloc-

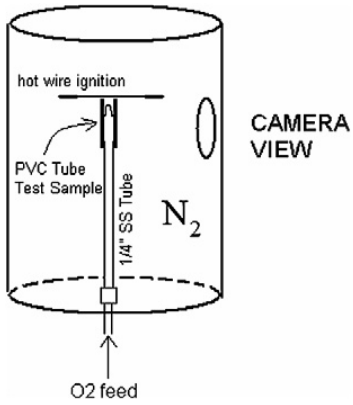

Fig. 2. Schematic of combustion chamber for vertical tube orientation.

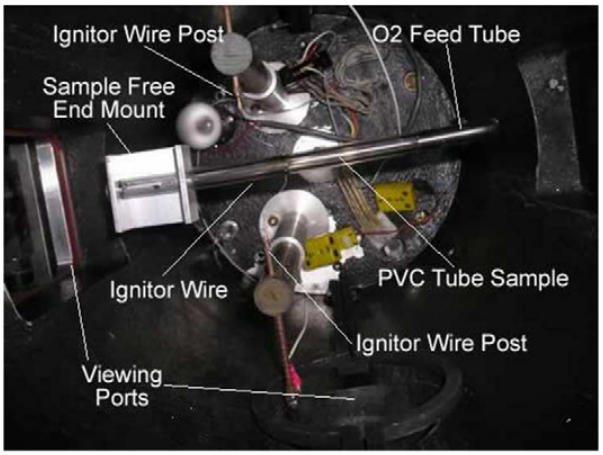

Fig. 3. Photograph of combustion chamber for horizontal tube orientation. View is from above with the top lid of the combustion chamber removed.

ity (40 cm/s) to establish a propagating fire line. The flow rate was reduced and the flame progression monitored. Below opposed-flow velocities of 3 cm/s, the fire line broke into individual flamelets, whose spacing increased with decreasing flow velocities. Extinction was observed for opposed-flow velocities below 0.5 cm/s.

The goal of the present investigation is to report experimental results that compare the opposed-flow flame spread rates in normal and microgravity. The buoyant regime for the 6.35-mm-inner-diameter tube is chosen for study as the largest tube that did not exhibit an inflection point. This diameter is also large compared to that below which curvature effects were considered important in PVC (Fig. 1) and PMMA [14]. The possibility of developing a terrestrial-based test for screening materials is considered, as are the implications to surgical fire safety.

2. Experimental

The tests were conducted in the 2.2-s drop tower at the NASA Glenn Research Center. A general purpose rig consisting of a 25.4-cm-inner-diameter, 50.4-cm-inner-height cylindrical chamber and instrumentation was used, similar to that described by Olson [13]. A schematic of the test apparatus is shown in Fig. 2 and a photograph (with the horizontal setup) is shown in Fig. 3. The chamber was filled with nitrogen to the test pressure. The basic experiment consists of flowing oxygen (stored in a 75-cc cylinder on the rig) through a tube sample, igniting it with a hot wire in normal gravity, and dropping the rig after a flame is established (propagating toward the oxygen source) to observe microgravity effects. Two opposed-flow flame orientations were studied: horizontal and vertical (downward spreading). All tests were conducted using 0.635-cm-inner-diameter, 0.953-cm-outer-diameter clear polyvinyl chloride (PVC) tubing manufactured by New Age Industries (Product 1101149—Clearflo). This plasticized PVC tubing was used, as it provides direct visual observation of the flame, closely resembles the form and composition of endotracheal tubes used in surgery, and was used in previous normal-gravity studies.

For the vertical tests, a 14.5-cm-long 1/4″ stainless steel tube was attached to the port at the center of the chamber floor. An 18-cm-long tube sample was slipped over that tube and held in place at the free end. An igniter wire (10-cm-long 27 gauge Kanthal) was placed in a slit made in the tube sample (sufficiently far from the free end to prevent back diffusion of nitrogen). A nitrocellulose membrane filter (5.0-μm pore size) was cut into strips and used in some tests to enhance ignition. For the horizontal tests, oxygen was delivered through a stainless steel tube formed to provide for horizontal flow. Fully developed laminar flow is established for all cases. The opposed-flow velocity used for all plots is the average flow velocity. The maximum Reynolds number observed is approximately 100.

Two video cameras were mounted on the rig with right-angle views. A wide-angle view was used primarily to measure the flame spread rate. A closer view was used to observe more detailed flame structure, and only provided useful results for vertical flames. Shutter speeds were adjusted in an attempt to improve the quality of the images. Flames were generally brighter as the opposed-flow velocity increased, requiring higher shutter speeds. A light source on the floor of the chamber was turned on and off at different times to alter the image quality or to provide an event signal (such as the start of a drop).

The video was digitized and the flame spread rate was determined using software developed at NASA Glenn [16]. Fig. 4 shows the results of a typical tracking in which the position of the leading edge is plotted

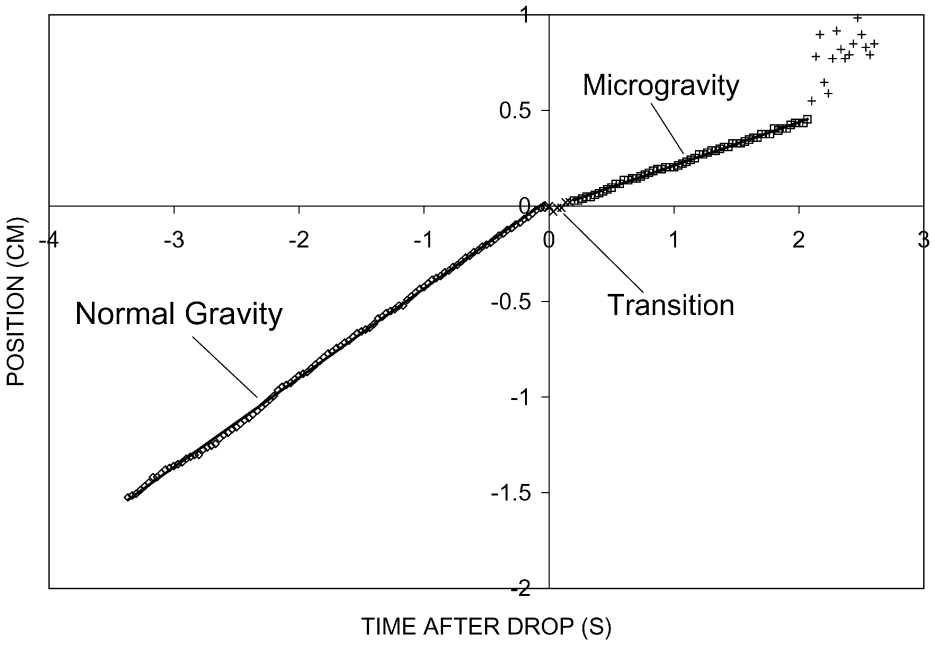

Fig. 4. Flame position plotted against time for a typical experiment using spotlight software. Test was a horizontal orientation with an opposed-flow velocity of 1.61 cm/s. The slopes from a linear fit are 0.47 cm/s before the drop and 0.23 cm/s after the drop.

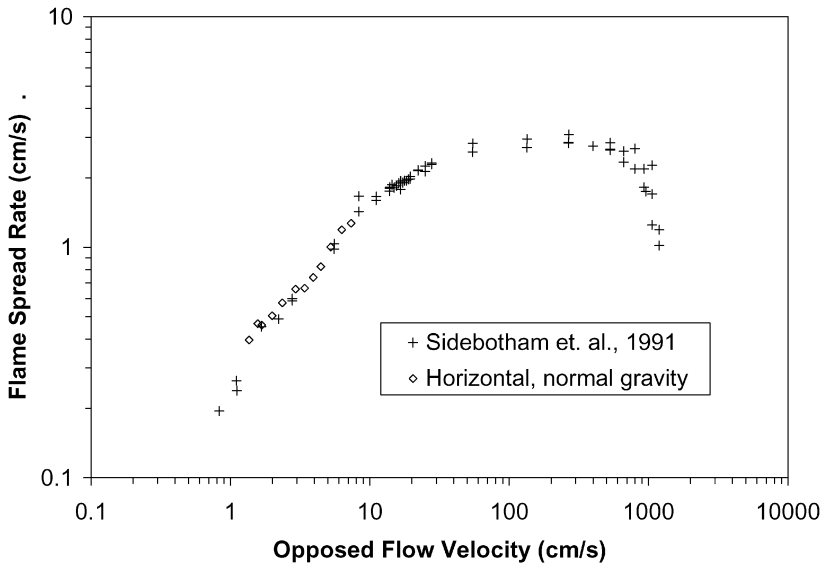

Fig. 5. Comparison of previous data obtained in normal gravity and present data during normal-gravity portion of the test. Flame spread rate is plotted against opposed-flow velocity.

as a function of time. Zero time and position correspond to the start of the drop. The chamber light was turned off for 0.2 s to signal the start of the drop, and the apparent location of the leading edge was affected, explaining the slight reversal in position during the transition period. In retrospect, this signal was unnecessary because the end of the drop is visible and it prevented precise analysis of the transition period. An estimate for the characteristic viscous decay time, $\tau_v = r^2/\nu$, within the tube is 0.22 s (for inner radius $r = 0.18$ cm and kinematic viscosity $\nu = 0.15\ \mathrm{cm}^2/\mathrm{s}$). In all cases, the flame spread rate abruptly changes to a new value within this time frame (even as the flame shape continues to adjust throughout the entire 2.2 s of the drop for some cases). The scattered points at the end of the test indicate the rig being brought to rest.

3. Results

3.1. Flame spread rate

Fig. 5 shows a comparison of the present results with the corresponding test performed previously in

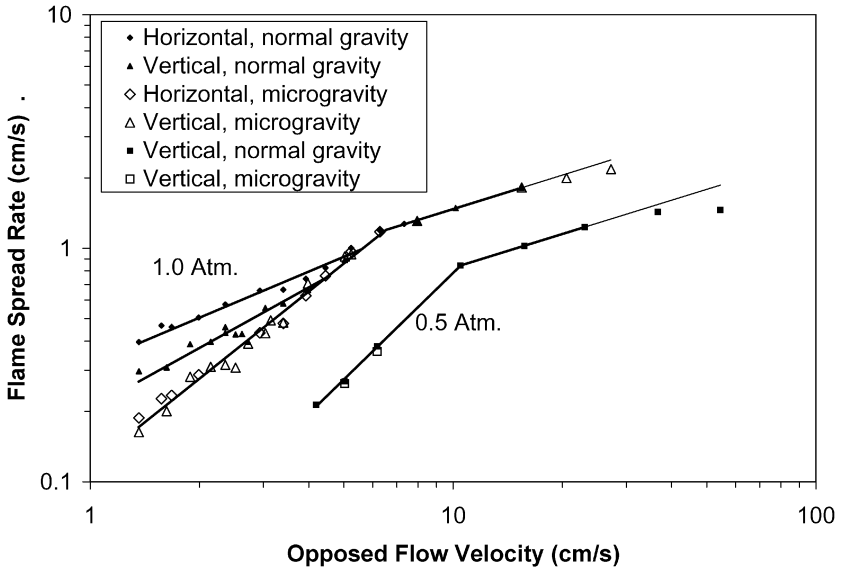

Fig. 6. Flame spread rate as a function of opposed-flow velocity for all tests conducted for this study.

Table 1
Power law fits to flame spread rate data $V_{\text{flame}} = AV_{O_2}^{n}$

Gravity level	Orientation	Pressure	Flow range	A	n
Micro	Combined data	1 atm	1.4–6.3 cm/s	0.117	1.24
Normal	Vertical	1 atm	1.4–4.5 cm/s	0.214	0.82
Normal	Horizontal	1 atm	1.4–5.6 cm/s	0.327	0.62
Micro	Combined data	1 atm	6.3–15.4 cm/s	0.484	0.48
Normal	Vertical	0.5 atm	4.2–10.5 cm/s	0.0239	1.52
Normal	Vertical	0.5 atm	10.5–23.0 cm/s	0.273	0.48

normal gravity for horizontal flame spread. The agreement is excellent, except for the low-flow limit of flame spread. The low-flow limit in the present study occurs at an opposing flow velocity of 1.36 cm/s (with a flame spread rate of 0.40 cm/s), while the prior study exhibits a limit at a flow velocity of 0.83 cm/s (with a flame spread rate of 0.20 cm/s). There is no clear explanation for this difference. Several attempts to ignite flames at a flow velocity of 1.30 cm/s were made using multiple contact points and electrical current pulses through the wire. A flame would establish near the hot wire ignition point and extinguish as it propagated away. The major differences in the two experiments are the mode of ignition, the external environment, and a different batch of sample from the manufacturer. A pilot flame held at the free end was used in the previous study with unlimited time of application. The previous tests were conducted in a fume hood, the present test in a sealed chamber with nitrogen. Due to the discrepancy, the low-flow limit in the present study is considered a hot-wire ignition limit, not necessarily a flammability limit.

Fig. 6 shows the flame spread rates plotted against opposed-flow velocity for all tests conducted in the present study. Tests in normal gravity are shown as filled symbols and the corresponding microgravity test as open symbols. Table 1 lists results of power law fits to various segments of these curves.

For the microgravity tests, the flame spread rate is independent of orientation. For flow velocities less than 6.3 cm/s, the flame spread rate increases with opposed-flow velocity with a power of 1.24. At flow velocity 6.3 cm/s, there is an abrupt change in slope, and the flame spread rate increases with a power of 0.48 for flow velocities between 6.3 and 15.4 cm/s. The power law fit is extrapolated to a flow velocity of 20.4, the highest velocity tested.

Below an opposed flow of approximately 5 cm/s, there is a clear effect of buoyancy. At the low-flow limit (1.36 cm/s opposed-flow velocity), the horizontal, vertical, and microgravity flame spread rates are 0.40, 0.30, and 0.16 cm/s, respectively. The horizontal case has a lower power law exponent (0.65) than the vertical case (0.86), which is less than the microgravity case (1.24). The normal gravity curves merge with the microgravity curve at opposed-flow velocities of 4.5 and 5.6 cm/s for vertical and horizontal flames, respectively, with corresponding flame spread rates of 1.0 and 0.75 cm/s.

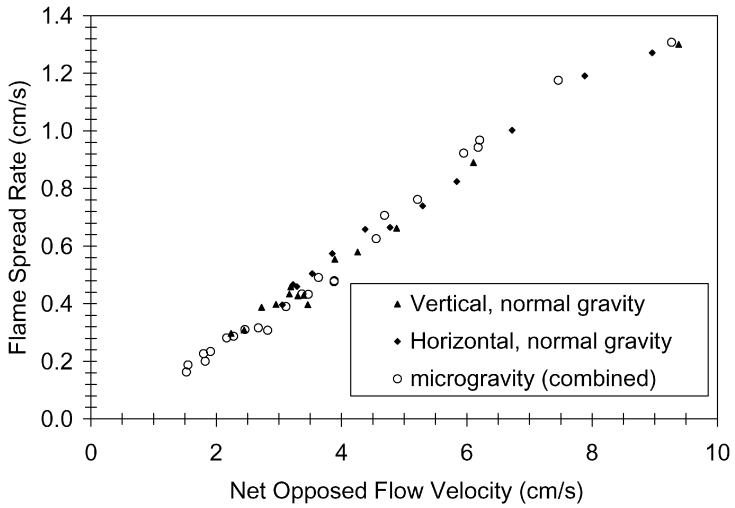

Fig. 7. Flame spread rate as a function of net opposed-flow velocity for atmospheric pressure horizontal and vertical tests in the buoyant regime. A buoyant flow of 1.5 cm/s for vertical flames and 2.5 cm/s for horizontal flames is added perpendicularly to the sum of the flame spread rate and opposed-flow velocity to define the net opposed-flow velocity observed by the flame.

There is a strong effect of pressure on flame spread rate. The curve generally has the same shape shifted to higher opposed velocities, with a modestly steeper slope in the low range (an exponent of 1.51) and virtually the same slope in the higher range. At reduced pressure, there is no effect of gravity for the two experiments tested. For the test at the lowest flow velocity, a normal-gravity flame was established and propagated at a steady rate for a distance of approximately 1.5 cm, at which point it extinguished. Therefore, there is no corresponding microgravity test for this point. The flame spread rate reported in normal gravity is that observed prior to self-extinction.

The induced buoyant flow velocity is estimated by defining a net opposed-flow velocity observed in flame coordinates. Fig. 7 shows the flame spread rate plotted against the net opposed-flow velocity for horizontal and vertical atmospheric pressure tests in normal and microgravity. The net opposed-flow velocity is defined as the sum of the flame spread rate and the oxygen velocity added vectorally to a fixed perpendicular buoyant flow velocity, namely,

$$V_{\text{net}} = (V_{\text{f}} + V_{\text{O}_2})\sqrt{1 + \frac{V_{\text{b}}^2}{(V_{\text{f}} + V_{\text{O}_2})^2}},$$

where V_{f} is the flame spread rate, V_{O_2} is the opposed-flow velocity, and V_{b} is the buoyant flow velocity. Fixed buoyant flow velocities of 1.5 cm/s for vertical flames and 2.5 cm/s for horizontal flames were selected to give the best agreement between the normal-gravity and microgravity tests.

3.2. Flame shape

The flame shape varied significantly depending on the flow rate of the oxidizer, the orientation, and the gravity level. The different flame shapes can be classified into three different general shapes. The transition from one flame type to another is gradual with increasing opposed-flow velocity, and does not appear to correlate with any change in flame spread behavior (for example, with the change in slope in Fig. 6).

Fig. 8 shows two photographs from the same horizontal flame test near the low-flow limit. Fig. 8a shows the flame in normal gravity, just prior to the drop, and Fig. 8b shows the flame in microgravity, near the end of the drop period. There are subtle differences in these flames, which will be addressed later. The flames travel from left to right against an opposed-flow velocity of 1.57 cm/s with flame spread rates of 0.47 and 0.23 cm/s, respectively. The chamber light was on for these images. When the chamber light is off, so that the only source of light is from the flame, only the blue portion of the flame is visible, which takes the shape of a classic flame spreading along a flat plate. With the chamber light on, a vapor cloud is visible that surrounds the flame and gives an indication of preheating and the flow field. It is plausible, though not proven, that the source of this vapor is the more volatile plasticizer in the material. The vapor cloud has a distinct leading edge, and interestingly, a distinct trailing edge. The shapes of these flames were analyzed manually using the spotlight software.

The leading edge of the vapor cloud gives an indication of a preheating length. Fig. 9a shows the measured length between the leading edge of the vapor cloud and the leading edge of the blue flame as a function of opposed-flow velocity for the horizontal normal- and microgravity flames. The preheating length decreases with opposed flow and is greater for microgravity flames than for normal-gravity flames. The preheat length adjusts to its new value within 0.5 s of microgravity, as shown in Fig. 9b, where

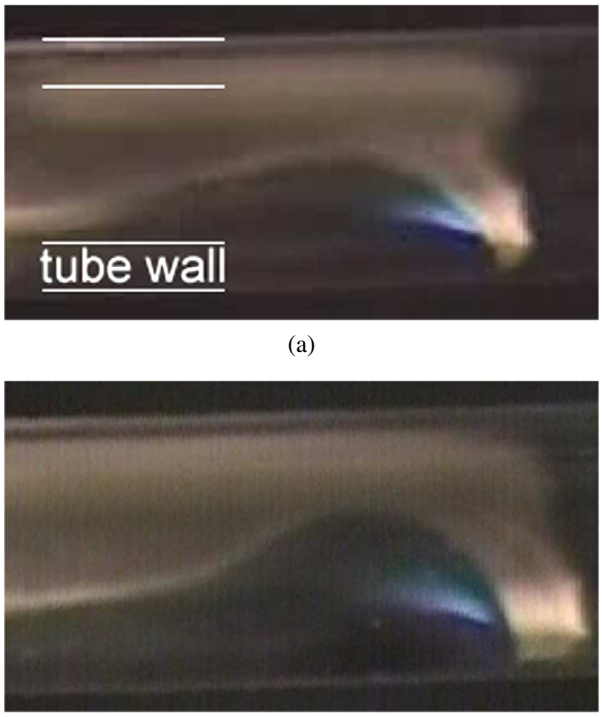

(a)

(b)

Fig. 8. Photographs of a typical one-sided flame (horizontal orientation) in normal gravity (a) and near the end of the microgravity time (b). Opposed-flow velocity is 1.57 cm/s (at atmospheric pressure) and flame spread rates are 0.47 and 0.23 cm/s for normal and microgravity, respectively. The tube wall locations are shown as white lines (6.35 mm i.d., 0.953 mm o.d.).

the preheat length is plotted against time, with time zero being the start of microgravity. The flame standoff distance, also shown in Fig. 9b, is not affected by gravity level and is on the order of 0.5 mm from the fuel surface. No attempts to account for light diffraction through the tube walls were made.

The shape of the vapor cloud also gives an indication of the velocity field. Fig. 10a shows the shape of the vapor cloud in normal gravity, after 1.1 s of microgravity, and after 2.2 s of microgravity. Fig. 10b shows a detail of the shape of the corresponding blue flames on an expanded length scale. The origin for these plots is taken to be on the original fuel surface at the axial position of the leading edge of the blue flame. There are three areas of interest for the vapor cloud: the leading edge at the fuel surface, the leading edge at the opposite side of the tube, and the trailing surface (between the cloud and the flame). Relative to the flame, the leading edge moves forward in microgravity, as discussed previously. On the opposite side of the tube, however, the location of the leading edge of the vapor cloud does not move relative to the flame. This result suggests that radiation from the vaporizing fuel surface is sufficient to begin preheating the opposite side to some degree. As the vapor cloud is swept toward the flame, it disappears at a sharp boundary (the trailing surface of the vapor cloud), suggesting that vapor droplets evaporate as they enter the higher temperature region. The shape of this surface changes gradually after the step from normal to microgravity, becoming rounder. In normal gravity, this surface is swept back more, suggesting a higher velocity as seen by the flame. There is a slight overlap of this surface with the flame surface in normal gravity, and it moves distinctly in front of the flame in microgravity.

There is little change in the shape of the blue flame with gravity level. The leading edge and lower surface are clear and distinct. These surfaces show little effect of gravity. The surface away from the fuel is less distinct. The generally thicker flame in microgravity may be related more to three-dimensional effects, for example, a change in the position of the leading surface behind the leading edge. This change is difficult to see from a single camera view. The shapes were obtained manually using tracker software, and the judgment of the location of the surface on the oxidizer side was more subjective than that for the distinct vapor surface on the fuel side.

This spreading flame type does not completely enclose the inner surface of the tube and shows a one-sided asymmetry. For horizontal tubes, the leading edge of the flame was always at the bottom of the tube, despite the fact that the ignition points were on the sides of the tube, and the nitrocellulose igniter strip, when used, was deliberately placed on the upper half of the tube. For vertical tubes, the same asymmetric flame spreading occurred, except that the leading edge usually (but not always) ran down at the point of one or the other ignition points where the ignition wire contacted the tube. Ignition and flame establishment were performed during normal gravity. The results of several drop attempts with ignition during microgravity were inconclusive as to whether there is a fundamental difference in the ignition process in normal and microgravity.

This one-sided asymmetric flame shape was observed for opposed-flow velocities less than 4.4 cm/s for horizontal flames and 2.7 cm/s for vertical flames (corresponding to flame spread rates of 0.82 and 0.4 cm/s, respectively).

For intermediate opposed flows (Figs. 11a and 11b for horizontal normal and microgravity flames, respectively), the flames exhibited a two-sided asymmetry; that is, there were two leading edges on opposite sides of the tube. This flame type was found for opposed-flow velocities of 5.2 to 6.3 cm/s for horizontal flames, and 3.0 to 4.0 cm/s for vertical flames (corresponding to flame spread rates of 1.00 to 1.19 cm/s and 0.56 to 0.66 cm/s, respectively). In horizontal tubes, the leading edges ran along the top and bottom despite the ignition points of contact being along the sides. During the flame establishment

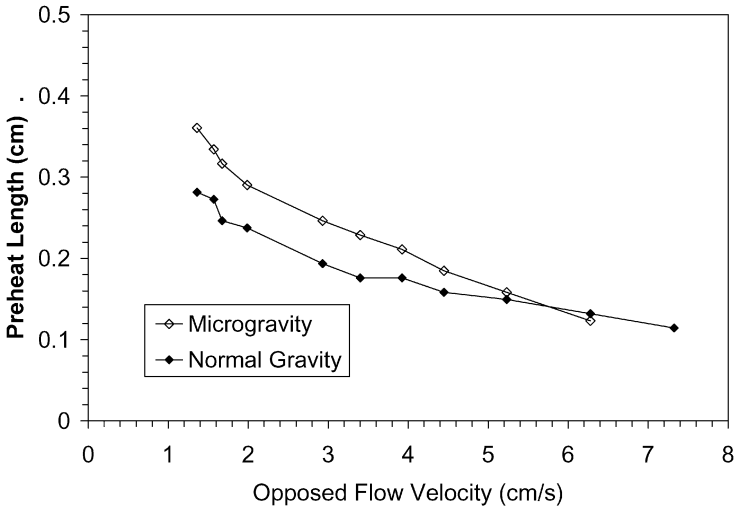

(a)

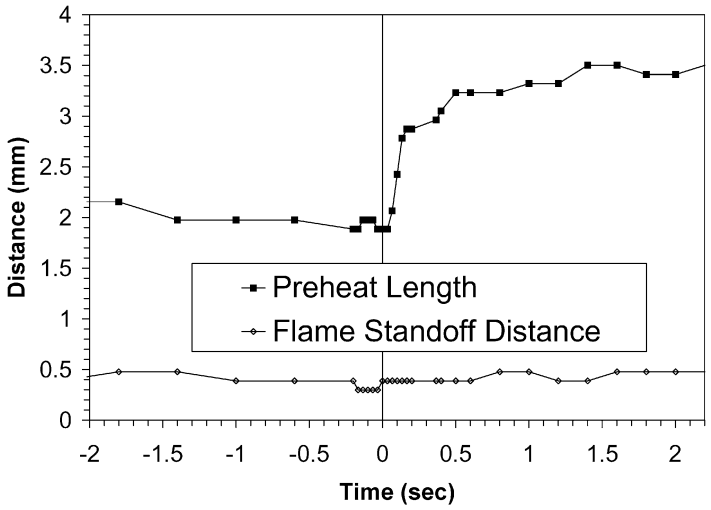

(b)

Fig. 9. (a) Preheat length (taken to be the distance between the leading edge of the vapor cloud and the leading edge of the blue flame) as a function of opposed-flow velocity for horizontal flames in normal and microgravity. (b) Preheat length and flame standoff distance as functions of time (with zero time coinciding with the start of the drop) for the test with opposed-flow velocity of 1.61 cm/s.

period in normal gravity, the leading edge at the bottom was always forward of the leading edge at the top (Fig. 11a). By the end of the microgravity portion of the test, the leading edges were at the same axial position (Fig. 11b).

Fig. 12 shows two orthogonal views of the same vertical normal-gravity flame taken from two different cameras. One view appears to be symmetric; the other shows the two leading edges. The leading edges are 90° from the point of ignition wire contact.

For higher opposed-flow rates (Fig. 13), the flame leading edge completely enclosed the inner surface of the tube, and there was no visible difference in flame shape in normal and microgravity, or for vertical or horizontal orientations. As the flow rate increased above a critical flow rate, the inner surface of the tube showed bubbling behind the leading edge. Soot formed on the fuel side of the flame (between the solid and the flame) and the flame resembled inverse diffusion flames, with an oxidizer jet surrounded by fuel.

4. Discussion

Bhattacharjee et al. [17] published a criterion for a fuel to be considered thermally thick. In the present case, the tube thickness is 1.6 mm for all tests. The critical thickness above which thermally thick flame spread occurs is given in [17] by

$$\tau_{cr} \sim \frac{\lambda_s}{\rho_g c_g V_g F} = 0.5 \text{ mm},$$

where λ_s is the thermal conductivity of the solid (assumed to be 0.09 W/m K), ρ_g is the gas phase density (1.2 kg/m^3), c_g is the gas phase specific heat

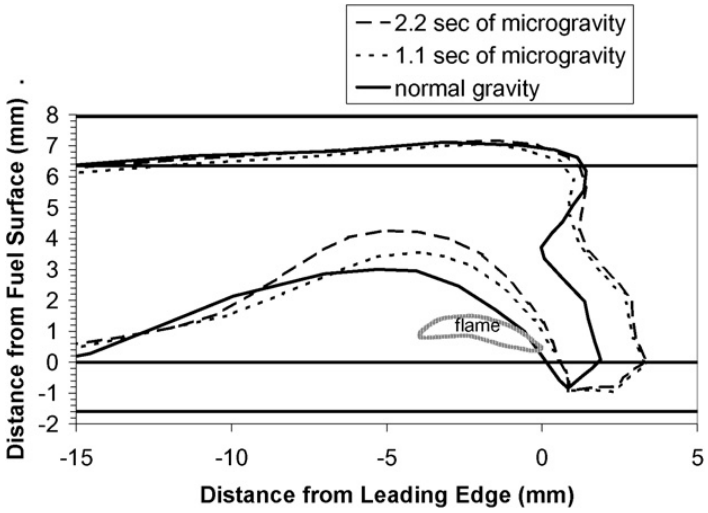

(a)

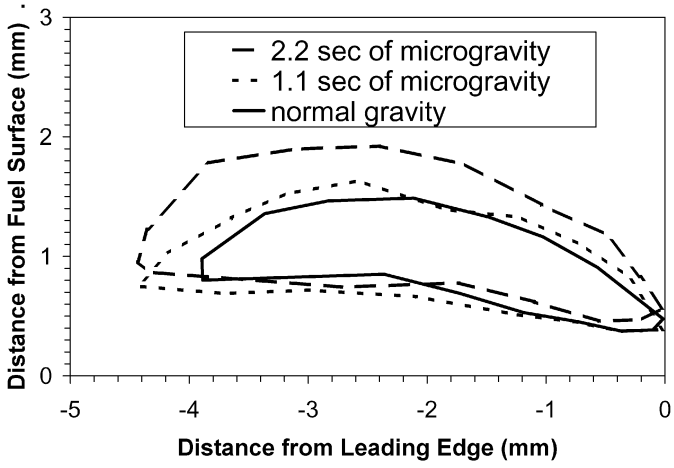

(b)

Fig. 10. Detailed shape of (a) vapor cloud and (b) flame for the horizontal flame with opposed-flow velocity of 1.61 cm/s. The origin is taken to be on the solid fuel surface at the axial position of the leading edge of the blue flame. Traces are shown for normal gravity, after 1.1 s of microgravity, and after 2.2 s of microgravity. No adjustments for tube wall optical effects are made.

(1000 J/kg K), V_g is the gas phase velocity (taken to be 0.0136 m/s, the lowest value for this study), and $F = (T_f - T_v)/(T_v - T_\infty)$ is a flame constant, where $T_f = 3091$ K and 3003 K is the equilibrium adiabatic flame temperature at 1.0 atm and 0.5 atm, respectively, $T_v = 530$ K is the solid vaporization temperature, and $T_\infty = 298$ K is the ambient temperature, and V_{O_2} is the opposed-flow velocity. The vaporization temperature is taken to be the spontaneous ignition temperature measured for this material [18]. Therefore, since the thickness of the tubes in this study is three times greater than the critical thickness, the flame spread is classified as thermally thick.

For flames spreading along solid fuels enclosed in a large ambient environment [10], low-flow flammability limits cannot be observed, since induced buoyant flows are greater than the low-flow limit that would be observed in a microgravity environment [11]. Hot gases generated from combustion are less dense than the environment, and a net upward force causes them to accelerate vertically. The rising gases are replenished by an induced flow of fresh ambient oxidizer. The length scale of this source flow field is greater than the length scale associated with the reaction zone. If the containment walls of the oxidizer are larger than this flow scale, then the ambient behaves as if it were infinite in extent. On the other hand, if the containment walls are within this scale, then the induced flow is impeded. The magnitude of the induced buoyant flow velocity was estimated from Fig. 7 to be 1.5 and 2.5 cm/s for vertical and horizontal normal-gravity flames, respectively. A plausible explanation for the difference is that for vertical flames, the rising hot gases induce a flow perpendicular to the fuel surface and forced opposed flow, and the primary effects are generally behind the leading edge. For horizontal flames, the rising hot gases induce a flow parallel to the fuel surface, which adds to the opposed flow seen by the leading edge. The magnitude of the buoyant flow velocity in these confined flames is an order

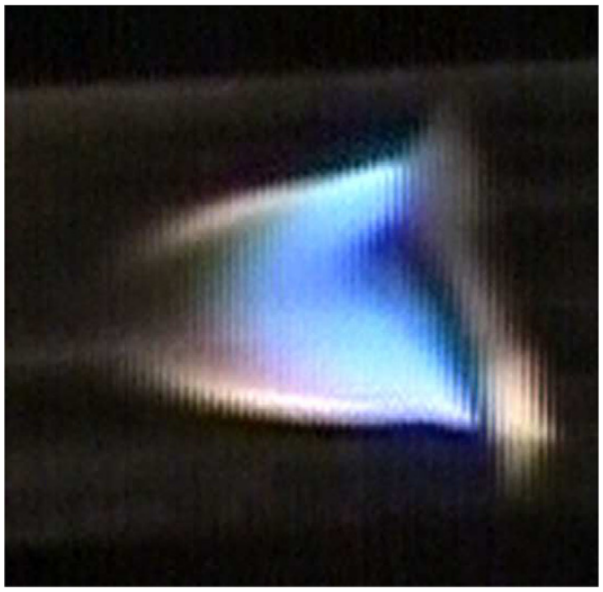

(a)

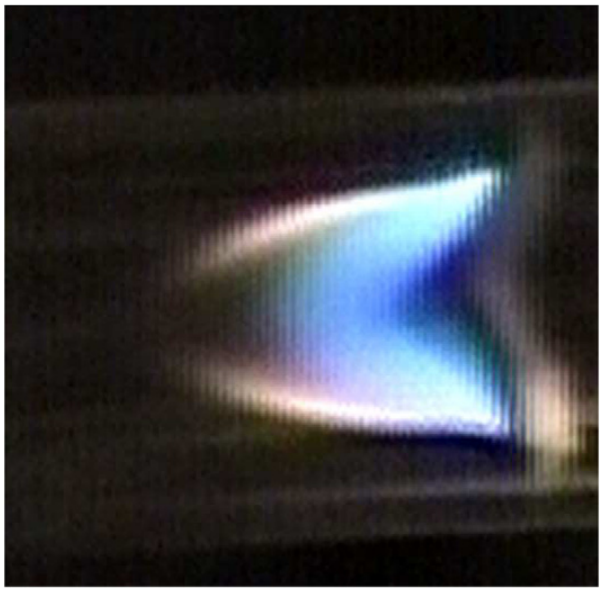

(b)

Fig. 11. Photographs of a typical two-sided flame (horizontal orientation) in normal gravity (a) and near the end of the microgravity time (b). Opposed-flow velocity is 5.4 cm/s (at atmospheric pressure) and flame spread rates are 1.0 and 0.97 cm/s for normal and microgravity, respectively.

of magnitude lower than that measured in unconfined opposed-flow flame spread [19].

Opposed-flow flame spread along the inner surface of tubes is a simple geometry that impedes buoyant flow without compromising the controlling physics near the leading edge. The low-flow ignition limit is the same in normal and microgravity. A similar geometry, used by Olson et al. [15], is to flow oxidizer through the space between two parallel plates, one of which is a test fuel. The other plate could be fuel or an inert shield. Either a cylindrical or a rectangular geometry can be used to study flame spread at low flow rates in ground-based experiments, with the vertically downward orientation giving somewhat greater buoyancy suppression. As shown in this study with pure oxygen, the effects of buoyancy are reduced, but not eliminated. However, the low-flow limit is a strong function of oxygen concentration. At lower oxygen concentrations, the low-flow limit occurs at much higher opposed-flow velocities [5,12], and buoyancy effects are likely eliminated at sufficiently low oxygen concentrations. At reduced pressure, the effect of buoyancy is eliminated in the present geometry. The opposed-flow velocity at the low-flow limit is much higher at reduced pressure, and the buoyant forces are lower due to the lower fluid density.

The horizontal orientation introduces a natural asymmetry in normal gravity because the gravity vector is perpendicular to the direction of opposed flow and flame spread. There is no such asymmetry for vertical tubes. There is some question as to whether the asymmetry for the vertical flames is due to an inherent asymmetry in the flame-spreading process, or to an asymmetry in the ignition process. Two methods were attempted to minimize the ignition asymmetry. An igniter strip was used, but could not fully eliminate the asymmetry. In the second method, ignition wire was passed four times through the tube, creating eight points of contact around the perimeter. The asymmetric flame spreading persisted in all these tests. Furthermore, not all flames ran along the line as it was ignited, but along some other line. It is concluded that the asymmetry for vertical flames is associated with the flame-spreading process, and the asymmetry of the ignition process merely determines a bias for the line along which the leading edge will run. This question could be more readily addressed in a normal-gravity experimental setup that allowed symmetric pilot ignition.

In a rectangular geometry [15], a propagating fire line was observed to break into flamelets as the flow was reduced, and the flamelet spacing increased with decreasing flow rate until extinction. The inside circumference of the tubes in the present study (20 mm) is comparable to the flamelet spacing observed, and the transition from flame line to wavelets occurs at similar opposed-flow velocities. Flamelets, a near-limit phenomenon, form when there is insufficient oxygen transport to the flame in the presence of inherent heat losses (conduction, surface radiation). The present confined cylindrical geometry yields flame asymmetries over a narrow range of near-quenching conditions reminiscent of flamelets in a rectangular geometry.

For the microgravity tests (Fig. 6), there is a clear and sudden change in flame spread rate power law slope at an opposed-flow velocity of 6.3 cm/s at atmospheric pressure (10.5 cm/s at 0.5 atm). This

(a)

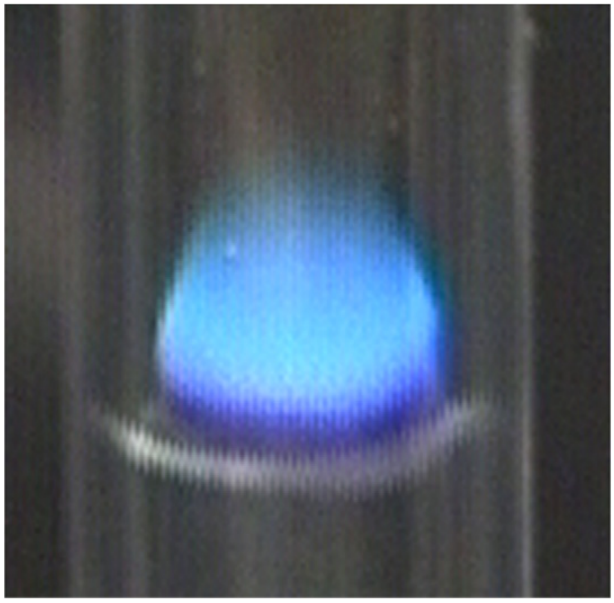

(b)

Fig. 12. Photographs of a normal-gravity two-sided flame (at 0.5 atm) with simultaneous orthogonal views. Opposed-flow velocity is 5.4 cm/s and the flame spread rate is 0.84 cm/s.

behavior suggests a change in controlling physical mechanism. Before the transition, the flame spread rate increases with flow velocity to a power greater than unity. It is plausible that radiative heat loss from the fuel surface plays an important role in this regime. Above this transition, the flame spread rate increases with the square root of flow velocity, as observed in microgravity studies of PMMA [20], although the effects of finite rate chemistry begin to reduce the slope soon after. While no further attempts are made to assess flame spread mechanisms in this paper, these data can serve as a basis for testing theoretical models of flame spread.

Should the need arise to conduct surgery in the head and neck area using high-energy surgical instruments during space flight, a method to minimize fire risk can be developed. The existence of a low-flow limit for this flame type provides a potential safety mechanism. Restricting the application of the surgical instrument to periods of breathing pause can be the basis for a protocol for such procedures. This method is not currently practiced in medicine because it involves real-time coordination between the anesthesiologist (administering breathing gas) and the precise timing of the application of the surgical device (laser or electrocautery) by the surgeon. While there have been attempts by manufacturers to produce endotracheal tubes that are laser-resistant, clear PVC tubing has advantages for the primary functions of anesthesia. However, the effect of instantaneous flow rate on

Fig. 13. Photograph of a normal-gravity symmetric flame (at 0.5 atm) showing microbubbles in the fuel corresponding to soot formation. Opposed-flow velocity is 11.8 cm/s and the flame spread rate is 1.23 cm/s.

the combustion characteristics of these flames is not well understood in the medical community. It is possible that systems to couple the anesthesia machine with high-energy surgical tools for space flight to reduce fire risk could be developed, and the technology subsequently introduced into ground-based medicine.

5. Conclusions

1. Opposed-flow flame spread velocities along the inner surface of 0.63-cm-i.d., 0.16-cm-thick PVC tubing in pure oxygen were measured in the NASA Glenn 2.2-s drop tower. Flames ignited in normal gravity were subjected to a step change in gravity, and steady propagation of both normal- and microgravity flames was thus obtained in a single test. The observed flame spread rate adjusted from its normal-gravity to a steady microgravity value within 0.2 s, while the shape of low-opposed-flow flames continued to adjust throughout the 2.2 s of microgravity.
2. Buoyant velocities of 2.5 and 1.5 cm/s for horizontal and vertical (downward) flame spread, respectively, were estimated at atmospheric pressure and normal gravity. These values are an order of magnitude lower than that for flame spread in an unconfined geometry.
3. Gravity level has no effect on flame spread rate above opposed-flow velocities of 4.5 and 5.6 cm/s for horizontal and vertical flames, respectively, at atmospheric pressure.
4. Flames could not be ignited below opposed-flow velocities of 1.4 cm/s, at which point flame spread rates are 0.39, 0.27, and 0.17 cm/s for horizontal, vertical, and microgravity (both orientations), respectively, at atmospheric pressure.
5. Flame spread in microgravity increases with a power law dependency with opposed-flow velocity, which suddenly changes from being greater than unity (1.24) to nearly square root (0.48) dependence at an opposed-flow velocity of 6.5 cm/s at atmospheric pressure.
6. There is no effect of gravity at a pressure of 0.5 atm. The opposed-flow velocity is 4.2 cm/s at the low-flow limit with a flame spread rate of 0.21 cm/s.
7. Flame asymmetries observed near the quenching limit are similar to flamelets observed in rectangular channels.
8. The risk of accidentally igniting PVC endotracheal tubes during surgery can be dramatically reduced by restricting the application of high-energy surgical tools to breathing pauses.

Acknowledgments

This paper is dedicated to the late Gerald L. Wolf, M.D., who brought this problem to the attention of the combustion community and worked tirelessly to educate the medical community on this and other fire safety risks. This work was supported by the NASA Faculty Fellowship Program (summer 2003). The contributions of the technical staff of the NASA Glenn 2.2-s drop tower are greatly appreciated. Special thanks to Peter Sunderland for help with all technical aspects of the project.

References

[1] S.J. Barker, J.S. Polson, Anesth. Anal. 93 (4) (2001) 960–965.
[2] J.I. Simpson, G.L. Wolf, Anesthesiology 65 (1986) 76–77.
[3] M.E. Bruley, Qual. Safe. Health Care 13 (2004) 467–471.

[4] G.W. Sidebotham, G.L. Wolf, A Preliminary Investigation of Flame Spread in Endotracheal Tubes, in: Fall Technical Meeting of the Eastern States Section of the Combustion Institute, 1989.
[5] G.W. Sidebotham, G.L. Wolf, J.B. Stern, R. Aftel, ASTM STP 1111, American Society for Testing and Materials, Philadelphia, 1991, pp. 168–178.
[6] G.L. Wolf, G.W. Sidebotham, J.B. Stern, Laryngoscope 104 (7) (1994) 874–879.
[7] NASA Technical Standard, NASA-STD-3001, vol. 1, 2007, Washington, DC, p. 44.
[8] H. Doerr, W.B. Murray, M. Cuttino, T.J. Broderick, ITACCS 16 (1) (2006) 26–30.
[9] J.B. Stern, An Experimental Study of Flame Spread within PVC Tubes with Application to the Endotracheal Tube Fire Problem, Masters thesis, The Cooper Union for the Advancement of Science and Art, New York, NY, 1990.
[10] A.C. Fernandez-Pello, S.R. Ray, I. Glassman, Proc. Combust. Inst. 18 (1981) 579–587.
[11] I.S. Wichman, Prog. Energy Combust. Sci. 18 (1992) 553–593.
[12] G.W. Sidebotham, J.A. Cross, G.L. Wolf, ASTM STP 1197, American Society for Testing and Materials, Philadelphia, 1993, pp. 43–57.
[13] S.L. Olson, Combust. Sci. Technol. 76 (1991) 233–249.
[14] N. Hashimoto, S. Watanabe, H. Nagata, T. Totani, I. Kudo, Proc. Combust. Inst. 29 (2002) 245–250.
[15] S.L. Olson, F.J. Miller, I.S. Wichman, Combust. Theory Modelling 10 (2) (2006) 323–347.
[16] R. Klimek, T. Wright, Spotlight 1.2: Image Analysis Software, Manual available at http://exploration.grc.nasa.gov/spotlight/.
[17] S. Bhattacharjee, R. Ayala, K. Wakai, S. Takahashi, Proc. Combust. Inst. 30 (2005) 2279–2286.
[18] G.L. Wolf, J.G. McGuire, P.F. Nolan, G.W. Sidebotham, ASTM STP 1197, American Society for Testing and Materials, Philadelphia, 1993, pp. 57–66.
[19] T. Hirano, K. Sato, Proc. Combust. Inst. 15 (1975) 233–241.
[20] S.L. Olson, U. Hegde, S. Bhattacharjee, J.L. Deering, T. Tang, R.A. Altenkirch, Combust. Sci. Technol. 176 (2004) 557–584.